

# A Single-Step Route to Robust and Fluorine-Free Superhydrophobic Coatings via Aerosol-Assisted Chemical Vapor Deposition

Julie Jalila Kalmoni, Frances L. Heale, Christopher S. Blackman, Ivan P. Parkin, and Claire J. Carmalt\*



Cite This: <https://doi.org/10.1021/acs.langmuir.3c00554>



Read Online

ACCESS |



Metrics & More

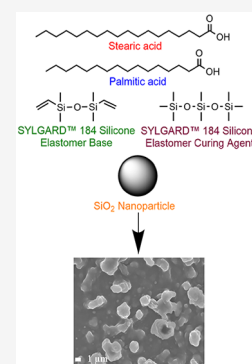


Article Recommendations



Supporting Information

**ABSTRACT:** Robust fluorine-free superhydrophobic films were produced from a mixture of two fatty acids (stearic acid and palmitic acid), SiO<sub>2</sub> nanoparticles, and polydimethylsiloxane. These simple and nontoxic compounds were deposited via aerosol-assisted chemical vapor deposition to provide the rough topography required for superhydrophobicity, formed through island growth of the aggregates. The optimum conditions for well-adhered superhydrophobic films produced films with a highly textured morphology, which possessed a water contact angle of  $162 \pm 2^\circ$  and a sliding angle of  $<5^\circ$ . Superhydrophobicity was maintained after ultraviolet exposure (14 days at 365 nm), heat treatment (5 h at 300 °C and 5 h at 400 °C), 300 tape peel cycles, and exposure to ethanol and toluene (5 h each).



## INTRODUCTION

Superhydrophobicity is a crucial property of materials for many large and small applications in which water adsorption can negatively influence functional performance. Examples include anti-icing coatings on airplanes, tuning the hydrophilicity of materials (e.g., cotton), and creating water resistant fabrics.<sup>1,2</sup> Superhydrophobicity was first observed in lotus leaves where water droplets roll off of the leaf surface rather than wet it, taking dirt particles with them to improve their functional performance, i.e., light harvesting or leaf health.<sup>3,4</sup> Superhydrophobicity is induced by the microscopic bumps and air spaces across the leaf, while the waxy cuticle provides the low surface energy required.<sup>5,6</sup> However, the widespread application of superhydrophobic coatings has been hindered due to their typically poor durability or robustness.<sup>7,8</sup>

The Wenzel and Cassie–Baxter models are the two main models used to describe superhydrophobicity.<sup>9</sup> Water droplets are more likely to stick to the surface when exhibiting Wenzel behavior as they penetrate protrusions from the surface of the materials. Cassie–Baxter behavior causes the water droplets to roll off or slip as the water droplets interact with the air pockets and peaks of the protrusions.<sup>10,11</sup> To replicate Cassie–Baxter behavior synthetically, both micro- and nanoscale roughness and a low-surface energy reagent are required.<sup>12</sup> The latter typically employs the use of toxic fluorinated polymers (due to their high durability and low affinity for water).<sup>13,14</sup>

Nonfluorinated alternatives, such as fatty acid-coated silica or metal nanoparticles, have been used to produce superhydrophobic coatings.<sup>15,16</sup> The properties of the fatty acids change depending on the length of their hydrophobic carbon chain, as confirmed by Heale et al., who fabricated hydro-

phobic slurries from innately hydrophilic silica nanoparticles dispersed in solutions of fatty acids.<sup>15,17</sup> Durable coatings were achieved only in the presence of an adhesive to bind the coating to the substrate. Daneshmand et al. reported stearic acid-coated Al<sub>2</sub>O<sub>3</sub> nanoparticles dispersed in either ethanol, methanol, or 2-propanol, which were then spray coated onto microscope glass substrates in a two-step process to ultimately produce a superhydrophobic film.<sup>18</sup> However, the use of a combination of fatty acids to achieve robust superhydrophobic films in a one-step process has not been studied.

The preparation of superhydrophobic films can be categorized into bottom-up approaches, top-down approaches, or a combination of both.<sup>5</sup> Top-down techniques involve starting with a bulk material, and examples include lithography, templating, and plasma etching.<sup>19–21</sup> In contrast, bottom-up methods involve using micro- and nanoscale units to build a structure using techniques, such as spin coating, sol–gel, and chemical vapor deposition (CVD).<sup>22–24</sup>

The aim of CVD is to ultimately form a thin solid film on a substrate via reactions in the gas phase to produce different gas-phase precursors.<sup>25,26</sup> Aerosol-assisted chemical vapor deposition (AACVD) is a type of CVD in which the precursor mixture (dissolved in a solvent) is aerosolised via a nebulizer/ultrasonic humidifier.<sup>24,27</sup> The carrier gas transports the

**Received:** February 28, 2023

**Revised:** May 4, 2023

**Table 1. Summary of the Experimental Conditions Used to Deposit the Superhydrophobic Thin Films via AACVD with a Flow Rate of 1 L/min and the Resulting Water Contact Angles (WCA)**

film	FAS C <sub>8</sub> /fatty acid used	mass of FAS C <sub>8</sub> /fatty acid used (g)	temperature of deposition (°C)	total deposition time (min)	WCA (deg)
PDMS/SiO <sub>2</sub>	–	–	360	40	159 ± 2
PDMS/SiO <sub>2</sub> /FAS	FAS C <sub>8</sub>	0.6	300	90	163 ± 2
PDMS/SiO <sub>2</sub> /SA	SA	0.6	300	90	145 ± 11
PDMS/SiO <sub>2</sub> /PA	PA	0.6	300	90	129 ± 3
PDMS/SiO <sub>2</sub> /SA+PA	SA and PA	0.6	300	90	162 ± 3
PDMS/SiO <sub>2</sub> /SA+PA/360	SA and PA	0.6	360	90	162 ± 2
PDMS/SiO <sub>2</sub> /SA+PA/400	SA and PA	0.6	400	90	129 ± 7
0.25PDMS/SiO <sub>2</sub> /0.25(SA+PA)	SA and PA	0.2	360	40	151 ± 7
0.5PDMS/SiO <sub>2</sub> /0.5(SA+PA)	SA and PA	0.4	360	40	161 ± 2
0.75PDMS/SiO <sub>2</sub> /0.75(SA+PA)	SA and PA	0.6	360	40	162 ± 2
1.0PDMS/SiO <sub>2</sub> /1.0(SA+PA)	SA and PA	0.8	360	40	163 ± 2
0.5PDMS/SiO <sub>2</sub> /0.5(SA+PA)/40 <sup>a</sup>	SA and PA	0.4	360	40	161 ± 2
0.5PDMS/SiO <sub>2</sub> /0.5FAS/40	FAS C <sub>8</sub>	0.4	360	40	161 ± 2
0.5PDMS/SiO <sub>2</sub> /0.5(SA+PA)/35	SA and PA	0.4	360	35	161 ± 2
0.5PDMS/SiO <sub>2</sub> /0.5(SA+PA)/30	SA and PA	0.4	360	30	146 ± 14
0.5PDMS/SiO <sub>2</sub> /0.5(SA+PA)/25	SA and PA	0.4	360	25	132 ± 8
0.5PDMS/SiO <sub>2</sub> /0.5(SA+PA)/10	SA and PA	0.4	360	10	112 ± 5

<sup>a</sup>This film is the same as 0.5PDMS/SiO<sub>2</sub>/0.5(SA+PA).

gaseous precursor to the heated reactor, causing the solvent to evaporate and precursors to react homogeneously or heterogeneously, eventually forming a solid film.<sup>24</sup>

If the precursor mixture is composed of polymers and/or silica nanoparticles, these particles diffuse from the heated carbon block toward the cooler glass top plate (substrate) by Brownian motion, a process described as thermophoresis.<sup>28</sup> AACVD involves the impaction of particles onto the substrate that are physisorbed, unlike conventional CVD that involves chemisorption.<sup>25,28</sup> AACVD is easily scalable, producing textured rough surfaces (a requisite for superhydrophobic films), and depends on only the solubility of the precursors (rather than their volatility).<sup>27</sup>

Previous reports on the formation of robust SiO<sub>2</sub> superhydrophobic thin films via AACVD have mainly involved the use of fluorinated polymers or layer-by-layer depositions to achieve well-adhered films that in some examples are also transparent.<sup>12,29</sup> Here, durable superhydrophobic thin films were prepared via a single-step AACVD route using SiO<sub>2</sub> nanoparticles in combination with either nonfluorinated or fluorinated polymers (for comparison). Their durability was achieved by using a combination of stearic acid and palmitic acid, which also engendered a dual-scale roughness, aiding superhydrophobicity. Even though polydimethylsiloxane (PDMS)/SiO<sub>2</sub> films are superhydrophobic, they are typically non-durable, powdery and can be wiped off the substrate with a tissue.

The water repellency, transparency, adherence, and self-cleaning properties were studied by adjusting the material combinations, loadings, polymer, and deposition temperatures to find the optimum conditions that could allow for the use of nonfluorinated species to create durable superhydrophobic films.

## EXPERIMENTAL SECTION

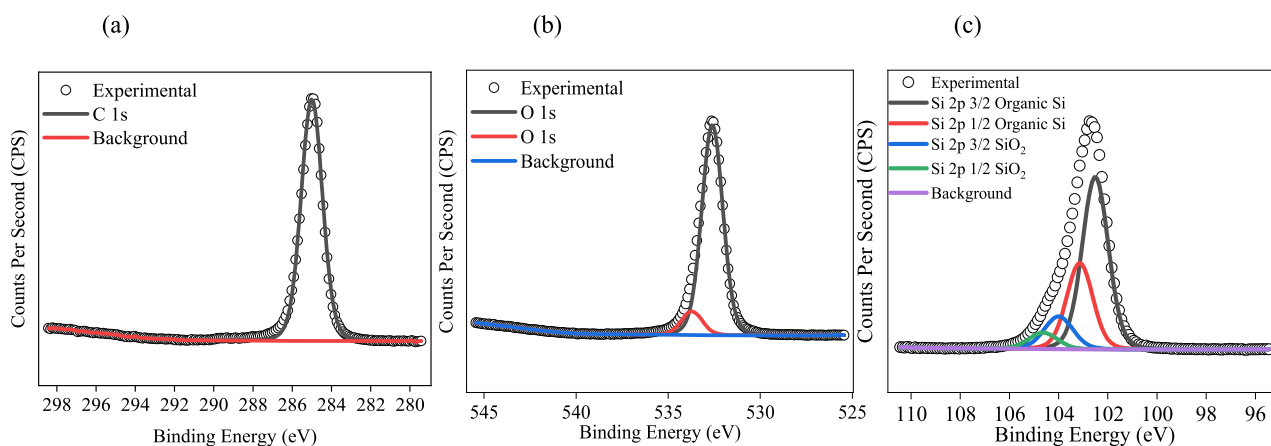
Vinyl-terminated PDMS, namely Sylgard-184 Silicone Elastomer Base, and its respective curing agent were purchased from Dow Corning. Aerosil OX50 fumed SiO<sub>2</sub> nanoparticles (NPs) were purchased from Lawrence Industries. Stearic acid (SA, reagent grade, 95%), palmitic acid (PA, ≥99%), 1H,1H,2H,2H-perfluoroo-

tyltriethoxysilane (FAS C<sub>8</sub>, 98%), and ethyl acetate (laboratory grade) were purchased from Sigma-Aldrich. Details of the various combinations used are described in Table 1. N<sub>2</sub> (99.99%) was supplied by BOC. SiO<sub>2</sub> barrier-coated float glass was provided by Pilkington NSG and cut into 150 mm × 40 mm × 3 mm pieces for AACVD.

**Synthesis of Superhydrophobic Coatings Using FAS C<sub>8</sub>, Stearic Acid, Palmitic Acid, or a Combination of Both Fatty Acids.** Sylgard-184 (0.60 g), its respective curing agent (0.06 g), FAS C<sub>8</sub> or palmitic acid or stearic acid or a 50:50 mixture of stearic acid and palmitic acid (0.6 g), and ethyl acetate (60 cm<sup>3</sup>) were mixed for 5 min. OX50 SiO<sub>2</sub> NPs (0.25 g) were then added to the precursor solution and mixed vigorously for an additional 20 min. Subsequently, the film precursor mixture was deposited on barrier-coated float glass in a bottom-down heating configuration where depositions occurred on the glass top plate (substrate). The graphite heating block possessed a Whatmann cartridge heater, which was regulated using a Pt–Rh cartridge heater. This setup was enclosed in a cylindrical quartz tube. Once the desired deposition temperature of 300 °C was reached, a piezoelectric ultrasonic humidifier was used to generate an aerosol that, with the N<sub>2</sub> carrier gas (1 L min<sup>-1</sup>), traveled through to the heated chamber for 40 min. Then, additional ethyl acetate (30 cm<sup>3</sup>) was added to the precursor mixture and left to deposit for an additional 30 min. Later, more ethyl acetate (20 cm<sup>3</sup>) was added to the precursor mixture but left to deposit for 20 min, with a total deposition time of 1.5 h. At the end of the deposition, the reactor was left to cool under a flow of nitrogen until the temperature was <100 °C. The coated glass top plate (substrate) was then handled in air. The obtained films were denoted as PDMS/SiO<sub>2</sub>/FAS, PDMS/SiO<sub>2</sub>/SA, PDMS/SiO<sub>2</sub>/PA, and PDMS/SiO<sub>2</sub>/SA+PA (where FAS is 1H,1H,2H,2H-perfluorooctyltriethoxysilane, SA is stearic acid, and PA is palmitic acid).

**Effect of Deposition Temperature.** The procedure described above was repeated using Sylgard-184 (0.60 g), its respective curing agent (0.06 g), a 50:50 mixture of stearic acid and palmitic acid (0.6 g), OX50 SiO<sub>2</sub> NPs (0.25 g), and ethyl acetate (60 cm<sup>3</sup>) at deposition temperatures of 360 and 400 °C for the film deposition experiments via AACVD. These films were denoted as PDMS/SiO<sub>2</sub>/SA+PA/360 and PDMS/SiO<sub>2</sub>/SA+PA/400.

**Effect of Changing the Concentration of All Reagents (except the SiO<sub>2</sub> NPs).** The concentrations of all of the reagents except the OX50 SiO<sub>2</sub> NPs were fractionally reduced by 75%, 50%, and 25% for Sylgard-184 (0.30 g), its respective curing agent (0.03 g), and a 50:50 mixture of stearic acid and palmitic acid (0.80 g). The



**Figure 1.** X-ray photoelectron data for the PDMS/SiO<sub>2</sub>/SA+PA film showing the (a) C 1s, (b) O 1s, and (c) Si 2p spectra.

masses and/or volumes of the OX50 SiO<sub>2</sub> NPs (0.25 g) and ethyl acetate (60 cm<sup>3</sup>) remained unchanged. The deposition time was 40 min with a temperature of 360 °C for all of the films in this study. The films were denoted as 1.0PDMS/SiO<sub>2</sub>/1.0(SA+PA), 0.75PDMS/SiO<sub>2</sub>/0.75(SA+PA), 0.5PDMS/SiO<sub>2</sub>/0.5(SA+PA), and 0.25PDMS/SiO<sub>2</sub>/0.25(SA+PA).

**Effect of Deposition Time.** The deposition time was varied (40, 35, 30, 25, and 10 min) with the temperature constant at 360 °C using the procedure outlined directly above. The films were denoted as 0.5PDMS/SiO<sub>2</sub>/0.5(SA+PA)/40, 0.5PDMS/SiO<sub>2</sub>/0.5(SA+PA)/35, 0.5PDMS/SiO<sub>2</sub>/0.5(SA+PA)/30, 0.5PDMS/SiO<sub>2</sub>/0.5(SA+PA)/25, and 0.5PDMS/SiO<sub>2</sub>/0.5(SA+PA)/10.

**Characterization.** The surface morphologies of the films were studied using JEOL JSM-6701F and JEOL JSM-7600F scanning electron microscopes with an accelerating voltage of 5–10 keV. All samples were vacuum sputtered with gold for 10 s prior to imaging to enhance the electrical conductivity of the films. The images were further analyzed using ImageJ version 1.52s. Fourier transform infrared spectroscopy (FT-IR) was performed using a Bruker alpha platinum attenuated total reflection (ATR) instrument, in the range of 400–4000 cm<sup>-1</sup>. Ultraviolet–visible (UV–vis) spectroscopy data were collected using a Shimadzu UV-2700 spectrophotometer in the range of 400–800 nm. X-ray photoelectron spectroscopy data were collected using a Thermo Scientific spectrometer with a monochromated Al K alpha source (8.3381 Å). The peaks were modeled using CasaXPS version 2.3.25, and binding energies were adjusted to adventitious carbon (285.0 eV). The Sq (root-mean-square height) of the films was determined by the Keyence VHX-S750E optical microscope at 1500× magnification, using a Gaussian filter type but no S-filter or L-filter.

A Kruss DSA 25E drop shape analyzer was used to determine the water contact angles (WCAs) of 10 deionized (DI) water droplets of ~5 μL across the central section of the films and calculated using ADVANCE version 1.14.3. The errors calculated are equivalent to one standard deviation. The sliding angles (SAs) were measured using the tilted drop method with a DI water droplet size of ~15 μL dispensed close to the middle of the substrate. The stage was already inclined before attempting any measurements. In all instances, the Young–Laplace equation was employed by the software to calculate the size of the angles. The contact angle hysteresis (CAH) was measured by subtracting the advancing contact angle (ACA) from the receding contact angle (RCA) via the sessile drop method.

**Durability. Ultraviolet Stability Test.** The samples were placed in a sealed box and exposed to ultraviolet (UV) light for 2 weeks with WCAs and SAs measured every 24 h (for the first 4 days and 7 and 14 days thereafter). This was carried out at room temperature with a UV emission wavelength of 365 nm and an intensity of 258 mW/cm<sup>2</sup> to replicate standard external UV irradiation.

**Polarity Stability Test.** The samples were immersed in two solvents of different polarities, ethanol and toluene, with WCAs measured at 1

h intervals for 5 h. Sliding angles were measured after immersion for 5 h.

**Heat Stability Test.** The samples were placed in a furnace at 300 °C for 5 h and, subsequently, for an additional 5 h at 400 °C. The WCAs were measured after each heat cycle, and SAs were measured at the end of the 10 h exposure.

**Tape Peel Test.** Scotch Magic Tape was stuck to and removed from the film 300 times, with WCAs measured after every 20 cycles and SAs measured after every 100 cycles.

**Pencil Hardness Test.** The Elcometer 501 Pencil Hardness Tester (Elcometer Ltd.) was used to obtain a hardness value based on a standard for ASTM D3363. Pencils with different hardnesses (6H–6B) were inserted into the pencil tester at a 45° angle to the surface and pushed across the film at a constant speed. The softest pencil was used with increasing hardness until a clear line was visible in the coating.

**Self-Cleaning. Self-Cleaning Tests.** The surfaces of the films were coated with gold glitter, and water droplets were manually dispensed directly onto the surface. Droplets of methylene blue dye were continuously dispensed directly onto the films, at a 20° angle. Photographs before, during, and after the test were taken, and all of the tests were carried out to determine the water repellency and self-cleaning ability of the films.

## RESULTS AND DISCUSSION

To investigate the effect of fluorinated versus nonfluorinated reagents for the formation of superhydrophobic coatings, AACVD of an ethyl acetate solution of SiO<sub>2</sub> NPs, polydimethylsiloxane (PDMS), and a long chain fluoroalkyl or alkyl species, including 1H,1H,2H,2H-perfluorooctyltriethoxysilane (FAS C<sub>8</sub>), stearic acid (SA), palmitic acid (PA), or a 50:50 SA/PA mixture, was studied at 300 °C. This combination of reagents enabled the formation of rough surfaces due to the presence of the SiO<sub>2</sub> NPs, along with hydrophobicity from the PDMS and FAS/SA/PA and durability from the polymer. Altering the long chain fluoroalkyl or alkyl species resulted in a change in hydrophobicity, as described below and given in Table 1. It is interesting to note that using a combination of SA and PA resulted in an increase in water contact angle to 162 ± 3° (compared to 145 ± 11° for SA and 129 ± 3° for PA).

The formation of a superhydrophobic film without using a fluorinated species was achieved via AACVD of PDMS, SiO<sub>2</sub> NPs, and a 50:50 SA/PA mixture in ethyl acetate at 300 °C (PDMS/SiO<sub>2</sub>/SA+PA film). This combination of reagents was therefore chosen to investigate the effect of changing the deposition temperature on the resulting film. These studies

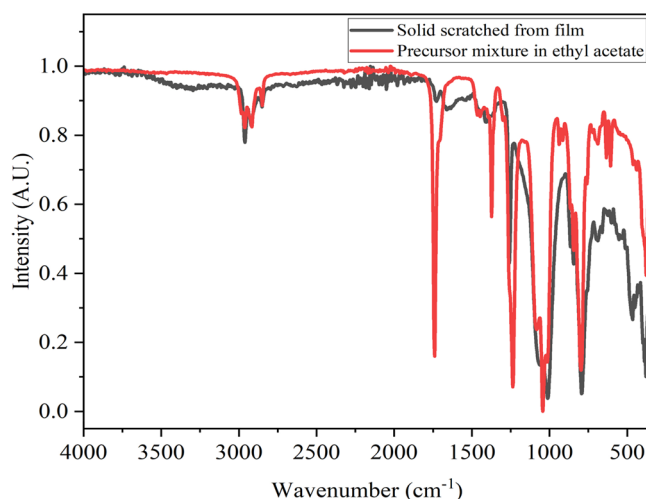
involved investigating the deposition of the same reagent mix at 360 and 400 °C, affording PDMS/SiO<sub>2</sub>/SA+PA/360 and PDMS/SiO<sub>2</sub>/SA+PA/400 films, respectively. The film deposited at 360 °C produced the most well-adhered superhydrophobic film, and hence, a temperature of 360 °C was used in all subsequent depositions. First, this involved studying the effect of the loading of PDMS and fatty acids in the precursor mixture. The concentrations of all of the reagents except the SiO<sub>2</sub> NPs were fractionally reduced by 25%, 50%, and 75%, relative to the unchanged film, producing  $x$ PDMS/SiO<sub>2</sub>/ $x$ (SA+PA) films ( $x = 0.25, 0.5, 0.75, \text{ and } 1.0$ ), as shown in Table 1. The final study involved varying the deposition time from the original 40 min to 35, 30, 25, and 10 min with the temperature kept constant at 360 °C and the same reagents (PDMS, a 50:50 SA/PA mixture, and SiO<sub>2</sub> NPs in ethyl acetate), as shown in Table 1. The variation of the deposition time was investigated at shorter deposition times rather than between 40 and 90 min because the films deposited at 40 and 90 min were very similar with similar WCAs. All resulting coatings were characterized using a range of techniques, including X-ray photoelectron spectroscopy (XPS), scanning electron microscopy (SEM), and FT-IR, and their functional properties were tested.

XPS was used to understand the surface chemistry of the resulting films, and the adventitious carbon peak at 285.0 eV was used as a charge reference. The XPS survey spectra of all films were consistent, indicating the presence of only C, O, and Si (except for the PDMS/SiO<sub>2</sub>/FAS film that also contains fluorine as expected). The XPS survey spectrum of a representative film, namely PDMS/SiO<sub>2</sub>/SA+PA, is shown in Figure S1. The XPS spectra for a PDMS/SiO<sub>2</sub>/FAS film are also given in Figure S2.

The deconvoluted C, O, and Si XPS spectra for all of the films were consistent, and a representative example is shown in Figure 1 for a PDMS/SiO<sub>2</sub>/SA+PA film. The C 1s spectra (Figure 1a) contain a peak at 285.0 eV, indicative of a C–O bridge between the Si–O bond of the NP and the carbon chain of the fatty acid, leading to the conclusion that the fatty acid attaches to the SiO<sub>2</sub> NP via the carboxyl group.<sup>30</sup> Figure 1b (O 1s) confirms the presence of SiO<sub>2</sub> (oxygen bound to Si) and organic C–O due to the peaks at 532.6 and 533.6 eV, respectively.<sup>17,31</sup> Figure 1c (Si 2p) proves the presence of organic silicon (102.5 eV) and SiO<sub>2</sub> (Si bound to O) at 104.0 eV, which is verified by the fact that O is bound to Si as in the O 1s spectrum, represented by the peak at 532.6 eV.<sup>32</sup> All peaks are in line with the literature.

The FT-IR spectra of all films incorporating fatty acids (SA, PA, or SA and PA) were similar regardless of the deposition conditions used, and a representative spectrum is shown in Figure 2. All films consisted of similar precursor mixtures (except when using FAS), with slight changes to the concentration of reagents or deposition conditions. Therefore, the individual peaks may pertain to more than one reagent due to the films having the same elements, C, H, O, and Si (except PDMS/SiO<sub>2</sub>/FAS), and no contaminants, as confirmed by XPS. The FT-IR spectra of the starting materials (OX50 SiO<sub>2</sub> NPs, PDMS, and its respective curing agent and the precursor mixture in ethyl acetate used to deposit the film) are presented in Figure S3. The FT-IR spectrum of the PDMS/SiO<sub>2</sub>/FAS film is shown in Figure S4.

All films displayed a strong stretch at  $\sim 1010 \text{ cm}^{-1}$  that could be assigned to the Si–O–Si asymmetric stretching vibrations. The sharp stretch at  $\sim 2960 \text{ cm}^{-1}$  was due to the Si–CH<sub>3</sub> group,



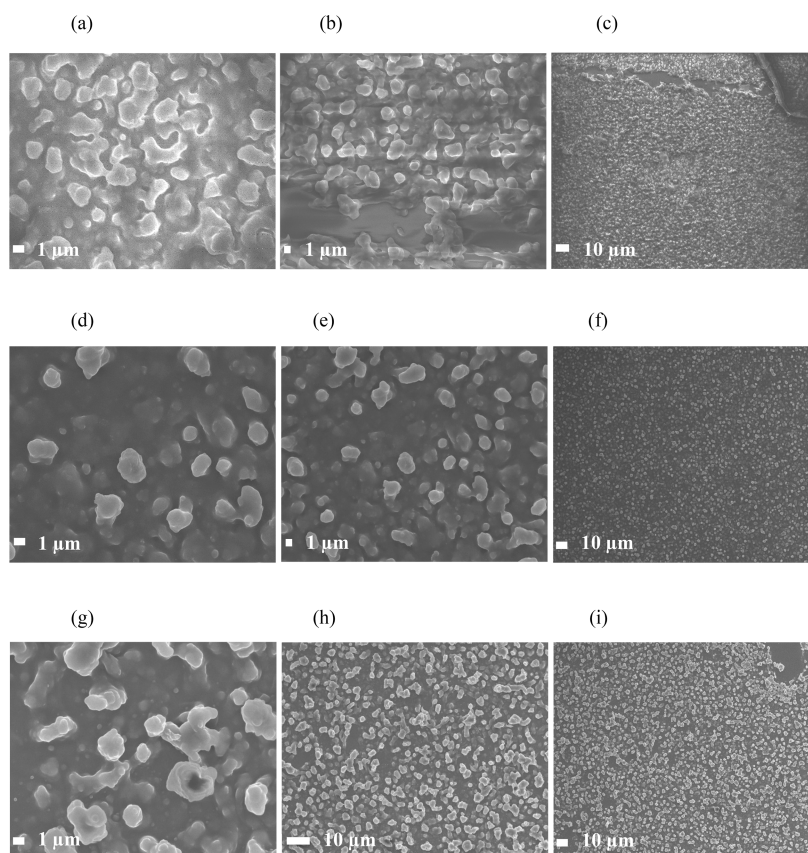
**Figure 2.** Fourier transform infrared (FT-IR) spectrum of the precursor mixture used to deposit the PDMS/SiO<sub>2</sub>/SA+PA film and the film itself (as a solid).

specifically the sp<sup>3</sup> C–H asymmetric stretch, indicative of the terminal –CH<sub>3</sub> groups of the PDMS. Similarly, all films contained at least one medium-intensity peak at 2910 or 2845 cm<sup>–1</sup>, indicative of the CH<sub>2</sub> asymmetric or symmetric bonds, respectively. This could be of the PDMS or CH<sub>2</sub> of the fatty acids.<sup>33</sup> The strong peak at  $\sim 1260 \text{ cm}^{-1}$  corresponded to the sp<sup>3</sup> C–H deformation.<sup>34</sup> The medium and strong peaks at 870 and 790 cm<sup>–1</sup>, respectively, were the stretching vibrations of CH<sub>3</sub>. The strong/broad peaks at  $\sim 1040$  and  $\sim 790 \text{ cm}^{-1}$  are indicative of the Si–O–Si asymmetric and symmetrical stretches, respectively, of PDMS and fumed SiO<sub>2</sub> NPs.<sup>35,36</sup>

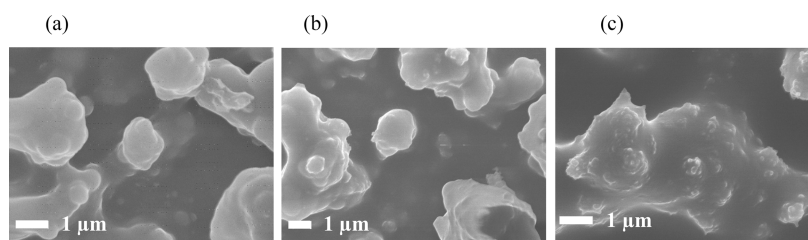
A small but sharp carboxylic acid C=O peak at approximately 1727 cm<sup>–1</sup> and the presence of the –OH stretch of the carboxyl group indicates the presence of the carboxyl groups of stearic acid and palmitic acid. Similarly, the positioning of this –OH group suggests that the fatty acids do not dimerize but remain as aliphatic chains.<sup>37</sup> Nevertheless, all peaks present were in close agreement with the literature.

High-magnification SEM images (Figure 3) indicated the presence of an interconnected network of particles that were nonspherical and nonuniform, which was greater when using a combination of fatty acids (PDMS/SiO<sub>2</sub>/SA+PA film). For example, SEM of the film using only palmitic acid (PDMS/SiO<sub>2</sub>/PA film) showed lower variability in the distance between the ends of the interconnected networks that ranged from 1.3 to 6.2  $\mu\text{m}$ . In contrast, the size range of the particles for the PDMS/SiO<sub>2</sub>/SA+PA film varied from 1.2 to 9.1  $\mu\text{m}$  with the lower limit relating to individual particles and the larger limit being the distance between the ends of the interconnected network.

Upon investigation of the WCA, it was found that coating the SiO<sub>2</sub> NPs with a single fatty acid (PDMS/SiO<sub>2</sub>/SA and PDMS/SiO<sub>2</sub>/PA films) resulted in variable hydrophobicity (WCAs of  $145 \pm 11^\circ$  and  $129 \pm 3^\circ$ ) and not superhydrophobicity. However, using a combination of two fatty acids (PDMS/SiO<sub>2</sub>/SA+PA film) led to superhydrophobicity across the entire film (WCA of  $165.3 \pm 1.6^\circ$ ), which was comparable to the WCAs from films deposited using the fluorinated polymer ( $163 \pm 2^\circ$ ). The differences in WCA are consistent with the differences in the observed morphologies of the films. The SEM images (Figure 3) confirmed that the



**Figure 3.** SEM images of films. Images a–c depict the morphology of PDMS/SiO<sub>2</sub>/SA (SiO<sub>2</sub> NPs coated with stearic acid). Images d–f represent PDMS/SiO<sub>2</sub>/PA (SiO<sub>2</sub> NPs coated with palmitic acid). Images g–i depict PDMS/SiO<sub>2</sub>/SA+PA (SiO<sub>2</sub> NPs coated with a 50:50 stearic acid/palmitic acid mixture).



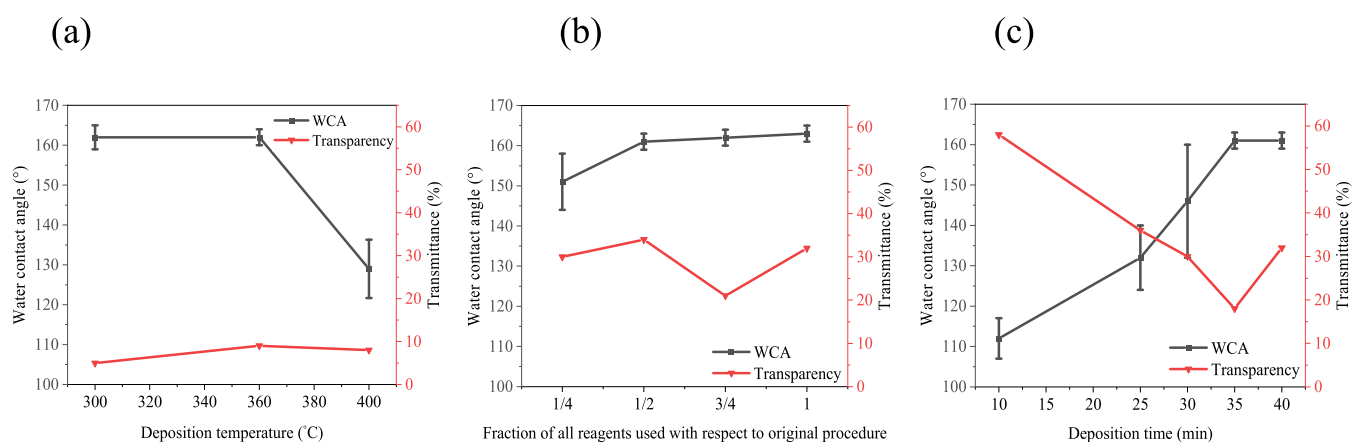
**Figure 4.** SEM images of the morphology of all films produced from PDMS and SiO<sub>2</sub> NPs coated with a 50:50 stearic acid/palmitic acid mixture but at (a) 300, (b) 360, and (c) 400 °C.

superhydrophobic films consisted of nano- and microscale particles of a range of sizes to create a textured morphology. An increase in the number of particles of different sizes led to greater roughness and hence increased the superhydrophobicity of the film confirmed by the *Sq* values of PDMS/SiO<sub>2</sub>/SA, PDMS/SiO<sub>2</sub>/PA, PDMS/SiO<sub>2</sub>/SA+PA, and PDMS/SiO<sub>2</sub>/FAS that are 0.69, 0.27, 1.32, and 1.35 μm, respectively. This was because air spaces could penetrate underneath the water droplet and hence increase the WCA. Some of the particles agglomerated to form microparticles or larger interconnected networks.

As AACVD of PDMS, SiO<sub>2</sub> NPs, and a 50:50 SA/PA mixture in ethyl acetate at 300 °C resulted in the formation of superhydrophobic films, this combination of reagents was used to investigate the effect of increasing the deposition temperature on the microstructure of the resulting film. The high-magnification SEM images for the films deposited at 300, 360, and 400 °C (Figure 4) show that the films formed via island

growth and the presence of spherical particles on the large, interconnected network of SiO<sub>2</sub> particles. In addition to the microparticles seen in all films, films grown at 360 and 400 °C have smaller particles on the elongated agglomerated structures, which were present in larger quantities in the latter. The small particles were more significant in the film deposited at 400 °C, which may have resulted due to fast evaporation of the precursor solvent (ethyl acetate), or the higher temperature could have led to faster curing of the Sylgard-184, leading to the formation of smaller microparticles.<sup>12</sup> Increasing the deposition temperature from 300 to 360 °C resulted in similar *Sq* values (1.32 and 1.24 μm) and no change in the WCA (Figure 5). However, increasing the temperature to 400 °C led to hydrophobicity, with a WCA of 129 ± 7°, which may be due to a decrease in surface roughness (*Sq* = 0.34 μm).

The effect of changing the concentration of the reagents in the precursor mixture was investigated. The concentrations of all of the reagents except the SiO<sub>2</sub> NPs were fractionally



**Figure 5.** Water contact angles for films deposited from PDMS, SiO<sub>2</sub> NPs, and a 50:50 SA/PA mixture (a) for the temperature study at 300, 360, and 400 °C, (b) by varying the concentration of  $x$ PDMS/SiO<sub>2</sub>/ $x$ (SA+PA) reagents ( $x = 0.25, 0.5, 0.75,$  and  $1$ ), and (c) by varying the deposition time (10, 25, 30, 35, and 40 min).

**Table 2. Summary of Water Contact Angles, Sliding Angles, Contact Angle Hysteresis, and Root-Mean-Square Heights for the 0.5PDMS/SiO<sub>2</sub>/0.5(SA+PA)/40 and 0.5PDMS/SiO<sub>2</sub>/0.5FAS/40 Films (with and without FAS C<sub>8</sub>, respectively)**

film	FAS C <sub>8</sub> /fatty acid used	deposition time (min)	water contact angle (deg)	sliding angle (deg)	contact angle hysteresis (deg)	Sq (μm)
0.5PDMS/SiO <sub>2</sub> /0.5(SA+PA)/40	50:50 stearic acid/palmitic acid mixture	40	163 ± 1	4 ± 1	14 ± 4	0.60
0.5PDMS/SiO <sub>2</sub> /0.5FAS/40	FAS C <sub>8</sub>	40	161 ± 2	4 ± 1	20 ± 9	0.66

reduced by 25%, 50%, and 75% relative to the unchanged film, producing  $x$ PDMS/SiO<sub>2</sub>/ $x$ (SA+PA) films ( $x = 0.25, 0.5, 0.75,$  and  $1.0$ ), as shown in Table 1. It was hypothesized that decreasing the concentration but keeping the deposition time the same may help in terms of decreasing the variability of the resulting coatings. The films deposited with different concentrations of reagents all had XPS, FT-IR, and SEM images similar to those of the films described above, as expected. A comparison of the WCAs for these films (Figure 5c and Table 1) shows little change in the WCA upon alteration of the concentration of the precursor mixture until the lowest concentration (25% of the original amount), which was  $\sim 12^\circ$  lower. This illustrates how the presence of the PDMS can enhance the superhydrophobicity. There was little change in transparency among these films; however, the lowest transmittance was observed for the 0.75PDMS/SiO<sub>2</sub>/0.75(SA+PA) film. This could be because film thickness can be difficult to control via AACVD, and hence, different areas of the resulting film may have different thicknesses.

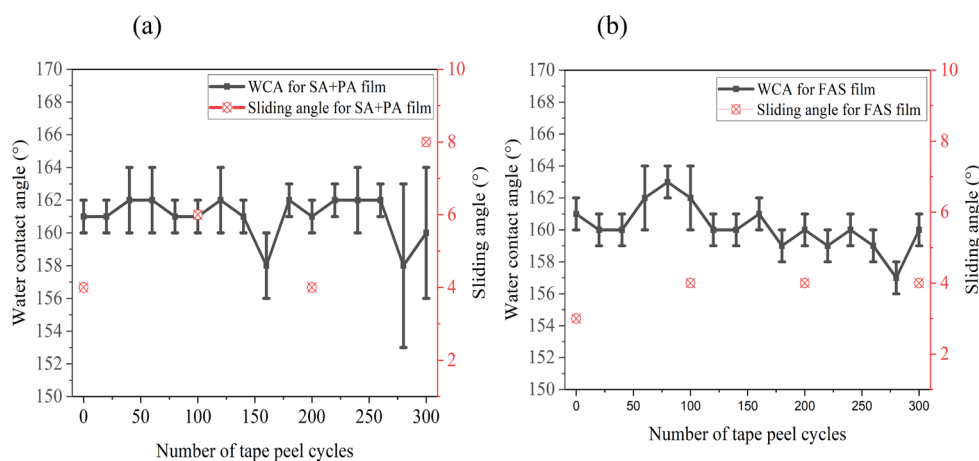
The deposition time was varied (40, 35, 30, 25, and 10 min) to explore its effect on the film's hydrophobicity, thickness, and transparency. The temperature was kept constant at 360 °C, and PDMS, a 50:50 SA/PA mixture, OX50 SiO<sub>2</sub> NPs, and ethyl acetate were used in each experiment. Analysis of the resulting films (XPS and FT-IR) shows that they were similar to the films described above. However, the SEM images indicate that as the deposition time was reduced, this led to less coverage and more porosity, which can be used to explain changes in hydrophobicity.

As shown in Figure 5c, a link between reducing the deposition time and the level of hydrophobicity was observed. The longer the deposition time, the more hydrophobic the film, with water contact angles ranging from hydrophobic (WCA of  $112^\circ$ ) at the shortest deposition time (10 min) to superhydrophobic (WCA of  $161^\circ$ ) at 35 min.

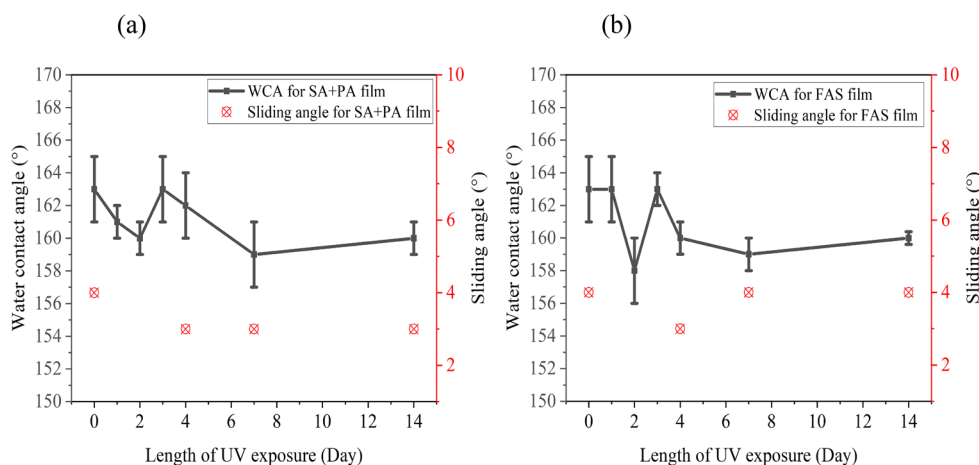
Superhydrophobicity and transparency are competing variables. As the WCA increases through a rougher and more complex morphology, the transparency decreases, which is evident in all of the films. A lower transmittance was observed for the PDMS/SiO<sub>2</sub>/SA (5%) and PDMS/SiO<sub>2</sub>/SA+PA (5%) films, relative to the PDMS/SiO<sub>2</sub>/PA (12%) film, and this is supported by the SEM images (Figure 3), which shows denser particles making the penetration of visible light difficult. The slight variations in transmittance of the films across the studies could be due to differences in the size of the particles, hence, their scattering with visible light, density of particles per unit area, and film thickness. The transmittance varied with deposition time due to the thickness of the film. Reducing the deposition time to 10 min created a thin film with a %T of  $\sim 60$ , although the resulting film was hydrophobic and not superhydrophobic.

**Functional Testing.** The optimum film of all of the different studies was 0.5PDMS/SiO<sub>2</sub>/0.5(SA+PA)/40 deposited at 360 °C because it was a well-adhered film with a high WCA. Therefore, this film was chosen to investigate the functional properties. For the purpose of comparison, the 0.5PDMS/SiO<sub>2</sub>/0.5FAS/40 film (a fluoroalkylsilane equivalent) was also studied. Images of the microstructure of the 0.5PDMS/SiO<sub>2</sub>/0.5FAS/40 film are shown in Figure S5. A comparison of the WCAs, CAH, and SAs shows that films deposited with SA and PA were superhydrophobic (Tables 1 and 2). The 0.5PDMS/SiO<sub>2</sub>/0.5(SA+PA)/40 film had a WCA of  $163 \pm 1^\circ$ , which was similar to that of 0.5PDMS/SiO<sub>2</sub>/0.5FAS/40 ( $161 \pm 2^\circ$ ); however, robustness tests proved that combining fatty acids contributed to the overall durability of the films.

During the sliding angle tests, the water droplet ( $\sim 15$  μL) rolled off at  $4^\circ$  indicating water repellency. The high-contact angle hysteresis (CAH) for both films ( $>10^\circ$ ) indicates Wenzel type behavior (a homogeneous regime) as the water droplet



**Figure 6.** Water contact angles and sliding angles during 300 tape peel cycles for (a)  $0.5\text{PDMS}/\text{SiO}_2/0.5(\text{SA}+\text{PA})/40$  and (b)  $0.5\text{PDMS}/\text{SiO}_2/0.5\text{FAS}/40$ .



**Figure 7.** Water contact angles and sliding angles during UV irradiation for 14 days of (a)  $0.5\text{PDMS}/\text{SiO}_2/0.5(\text{SA}+\text{PA})/40$  with a 50:50 SA/PA mixture and (b)  $0.5\text{PDMS}/\text{SiO}_2/0.5\text{FAS}/40$  with FAS  $\text{C}_8$ .

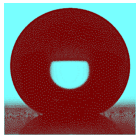
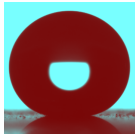

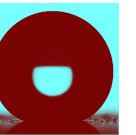
sticks to the surface and penetrates the protrusions, limiting the ability of the water droplet to move across a horizontal surface.<sup>10,11,38</sup>

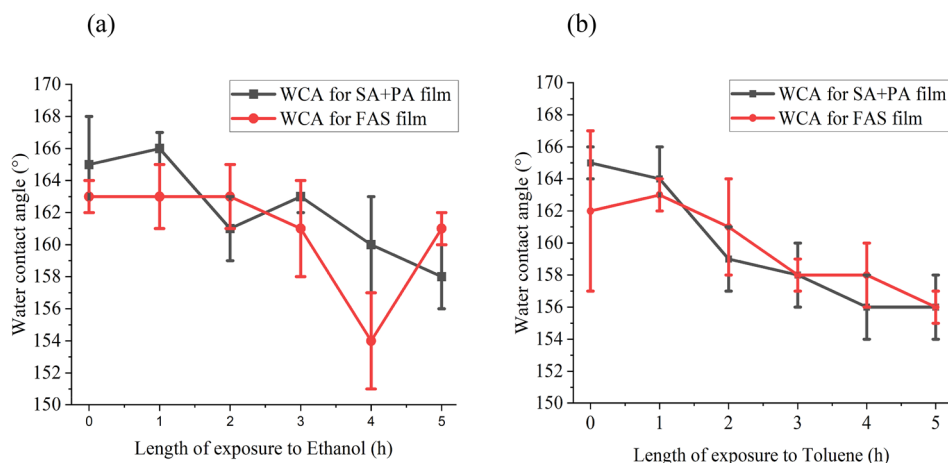
Several methods were pursued to determine the robustness of films such as UV irradiation, exposure to solvents of different polarities, and adhesive tape peel cycles. The adhesion of coatings to the glass substrates was evaluated via the tape peel test. Even after 300 cycles of the tape peel test, the WCAs of both films [with and without the fluoroalkylsilane (Figure 6)] were  $>150^\circ$ , and sliding angles were  $<10^\circ$ , indicating strong adhesion of the film to the substrate. For comparison, a PDMS/SiO<sub>2</sub> film underwent 20 cycles of the tape peel test. Before the test, it had a water contact angle of  $159 \pm 2^\circ$ , but after 20 cycles, this became  $147 \pm 2^\circ$ , indicating hydrophobicity and poor durability.

Figure 7 highlights the stability of  $0.5\text{PDMS}/\text{SiO}_2/0.5(\text{SA}+\text{PA})/40$  and  $0.5\text{PDMS}/\text{SiO}_2/0.5\text{FAS}/40$  films upon exposure to UV irradiation, which is known to oxidize the organic components, creating hydrophilic groups.<sup>39</sup> Nevertheless, even after UV exposure ( $\lambda = 365 \text{ nm}$ ), both films retained their superhydrophobicity throughout the 14-day cycle with WCAs of  $>155^\circ$  and some increase in sliding angle (although it is still  $<10^\circ$ ). Minimal changes are due to the chemical composition of the films; SiO<sub>2</sub> NPs and fatty acids are not photoactive and hence resistant to UV radiation.

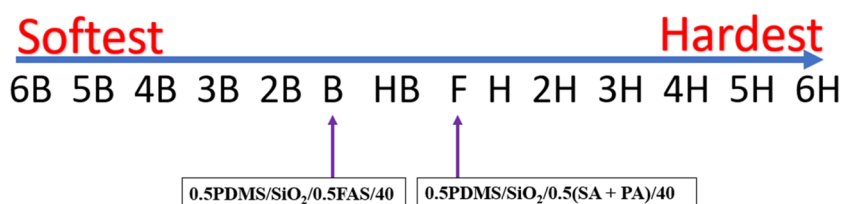
Table 3 gives the results of heat stability tests that showed both films maintained their superhydrophobicity following exposure at  $300^\circ\text{C}$  for 5 h. After exposure at  $400^\circ\text{C}$  for 5 h, the WCA for  $0.5\text{PDMS}/\text{SiO}_2/0.5\text{FAS}/40$  decreased to  $159^\circ$ .

**Table 3. Images, Water Contact Angle Measurements, and Sliding Angle Measurements for the  $0.5\text{PDMS}/\text{SiO}_2/0.5(\text{SA}+\text{PA})/40$  and  $0.5\text{PDMS}/\text{SiO}_2/0.5\text{FAS}/40$  Films after Heating at  $300^\circ\text{C}$  for 5 h and  $400^\circ\text{C}$  for an Additional 5 h**

	$0.5\text{PDMS}/\text{SiO}_2/0.5(\text{SA}+\text{PA})/40$ 50:50 ratio of SA + PA		$0.5\text{PDMS}/\text{SiO}_2/0.5\text{FAS}/40$ FAS $\text{C}_8$	
	After 5 h of $300^\circ\text{C}$ exposure	After 5 h of $400^\circ\text{C}$ exposure	After 5 h of $300^\circ\text{C}$ exposure	After 5 h of $400^\circ\text{C}$ exposure
WC A ( $^\circ$ )				
SA ( $^\circ$ )	N/A	1	N/A	7



**Figure 8.** Water contact angles for  $0.5\text{PDMS}/\text{SiO}_2/0.5(\text{SA}+\text{PA})/40$  and  $0.5\text{PDMS}/\text{SiO}_2/0.5\text{FAS}/40$  films during exposure for 5 h to (a) ethanol and (b) toluene.



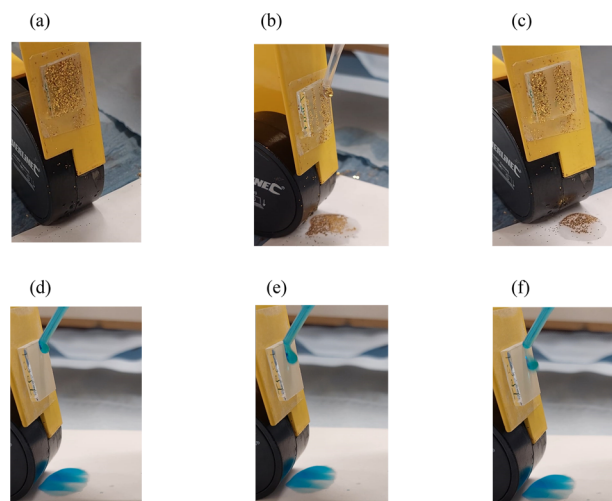
**Figure 9.** Measures of the hardness for  $0.5\text{PDMS}/\text{SiO}_2/0.5(\text{SA}+\text{PA})/40$  and  $0.5\text{PDMS}/\text{SiO}_2/0.5\text{FAS}/40$  films.

The opposite was observed for  $0.5\text{PDMS}/\text{SiO}_2/0.5(\text{SA}+\text{PA})/40$ , with WCAs reaching  $170^\circ$ , potentially due to the evaporation of excess ethyl acetate, chain diffusion of the hydrophobic carbon chain to the film's surface, or formation of organic compounds on the surface.<sup>40</sup>

Upon exposure to solvents of contrasting polarity (ethanol and toluene) for 5 h, the measured sliding angles were largely unchanged for both  $0.5\text{PDMS}/\text{SiO}_2/0.5(\text{SA}+\text{PA})/40$  and  $0.5\text{PDMS}/\text{SiO}_2/0.5\text{FAS}/40$  with the maximum change being a  $1^\circ$  reduction in sliding angle for  $0.5\text{PDMS}/\text{SiO}_2/0.5\text{FAS}/40$  after exposure to toluene for 5 h (Figure 8). There was a  $<10^\circ$  reduction in WCA in both films, which is likely due to strong physical attractions between the fatty acids coating the NPs and glass substrate in addition to the low surface energy of the PDMS and fatty acids.

The ability of the films to tolerate hardness was measured using an elcometer (Figure 9) with the robustness of the  $0.5\text{PDMS}/\text{SiO}_2/0.5\text{FAS}/40$  film being less than that of the  $0.5\text{PDMS}/\text{SiO}_2/0.5(\text{SA}+\text{PA})/40$  film due to the film's microstructure. Nevertheless, both films displayed reduced mechanical resistance relative to films with similar compositions deposited via other methods as AACVD involves the physisorption of the films onto the glass top plate (substrate) rather than chemisorption.<sup>25,28</sup>

Self-cleaning tests with  $0.5\text{PDMS}/\text{SiO}_2/0.5(\text{SA}+\text{PA})/40$  were performed at a tilt angle of  $20^\circ$ . Its self-cleaning ability was visualized by coating the surface with gold glitter and pipetting water droplets directly onto the film (Figure 10). As shown in Figure 10a, the water droplets slid off, readily clearing the glitter in its path, demonstrating its self-cleaning ability. In a stain test, multiple water droplets of methylene blue dye were pipetted on the surface to determine if it stained the films. The resultant films were dry and unstained due to the water's high surface tension and the coating's low surface energy.



**Figure 10.** Self-cleaning ability of the  $0.5\text{PDMS}/\text{SiO}_2/0.5(\text{SA}+\text{PA})/40$  film using gold glitter: (a–c) methylene blue dye and (d–f) both at a tilted angle of  $20^\circ$ .

## CONCLUSION

In this study, robust fluorine-free superhydrophobic films of PDMS, its respective curing agent,  $\text{SiO}_2$  NPs, and a 50:50 SA/PA mixture were deposited via AACVD using a one-pot precursor mixture. All reagents were nontoxic, successfully incorporated into the films, and had water contact angles  $>150^\circ$  regardless of the deposition conditions. The best film, deposited at  $360^\circ\text{C}$  for 40 min, displayed excellent mechanical durability after 300 tape peel cycles and retained superhydrophobicity after exposure for 5 h to solvents of contrasting polarities, heat exposure at  $400^\circ\text{C}$ , and UV irradiation for 14 days. The film also demonstrated self-cleaning abilities.



Previous research has demonstrated that when using AACVD, a fluoroalkylsilane or multiple depositions are required to produce superhydrophobic coatings.<sup>13,29,41</sup> This study has shown that a combination of two fatty acids can contribute to superhydrophobicity and increased robustness, hence providing a facile new route for producing nontoxic superhydrophobic coatings. Further work could involve improving the transparency of the films.

## ■ ASSOCIATED CONTENT

### SI Supporting Information

The Supporting Information is available free of charge at <https://pubs.acs.org/doi/10.1021/acs.langmuir.3c00554>.

X-ray photoelectron survey spectra and FT-IR spectra of films with SA/PA mixtures and FAS and SEM images of 0.SPDM/SiO<sub>2</sub>/0.5FAS/40 (PDF)

## ■ AUTHOR INFORMATION

### Corresponding Author

Claire J. Carmalt – Materials Chemistry Centre, Department of Chemistry, University College London, London WC1H 0AJ, U.K.; [orcid.org/0000-0003-1788-6971](https://orcid.org/0000-0003-1788-6971); Email: [c.j.carmalt@ucl.ac.uk](mailto:c.j.carmalt@ucl.ac.uk)

### Authors

Julie Jalila Kalmoni – Materials Chemistry Centre, Department of Chemistry, University College London, London WC1H 0AJ, U.K.

Frances L. Heale – Materials Chemistry Centre, Department of Chemistry, University College London, London WC1H 0AJ, U.K.; [orcid.org/0000-0002-0473-7128](https://orcid.org/0000-0002-0473-7128)

Christopher S. Blackman – Materials Chemistry Centre, Department of Chemistry, University College London, London WC1H 0AJ, U.K.; [orcid.org/0000-0003-0700-5843](https://orcid.org/0000-0003-0700-5843)

Ivan P. Parkin – Materials Chemistry Centre, Department of Chemistry, University College London, London WC1H 0AJ, U.K.; [orcid.org/0000-0002-4072-6610](https://orcid.org/0000-0002-4072-6610)

Complete contact information is available at: <https://pubs.acs.org/doi/10.1021/acs.langmuir.3c00554>

### Author Contributions

J.J.K. produced and characterized all films, and F.L.H. carried out initial studies in fabricating the FAS films. J.J.K. and C.J.C. wrote the initial draft of the manuscript with contributions from C.S.B. and I.P.P. The work was supervised by C.J.C., C.S.B., and I.P.P. All authors contributed to scientific discussions throughout the work.

### Notes

The authors declare no competing financial interest.

## ■ ACKNOWLEDGMENTS

J.J.K. is grateful to the EPSRC (EP/N509577/1 and EP/T517793/1) and UCL Chemistry for their funding and support. C.J.C., I.P.P. and F.L.H. also thanks Innovate UK (102541) and the Centre for Doctoral Training in Molecular Modelling and Materials Science for financially supporting this project (EPSRC grant EP/N510051/1).

## ■ REFERENCES

(1) Jiao, Y.; Zhang, T.; Ji, J.; Guo, Y.; Wang, Z.; Tao, T.; Xu, J.; Liu, X.; Liu, K. Functional Microtextured Superhydrophobic Surface with

Excellent Anti-Wear Resistance and Friction Reduction Properties. *Langmuir* **2022**, *38*, 13166–13176.

(2) Wang, T.; Hu, X.; Dong, S. A general route to transform normal hydrophilic cloths into superhydrophobic surfaces. *Chem. Commun.* **2007**, 1849–1851.

(3) Barthlott, W.; Neinhuis, C. Purity of the sacred lotus, or escape from contamination in biological surfaces. *Planta* **1997**, *202*, 1–8.

(4) Park, S.; Huo, J.; Shin, J.; Heo, K. J.; Kalmoni, J. J.; Sathasivam, S.; Hwang, G. B.; Carmalt, C. J. Production of an EP/PDMS/SA/AlZnO Coated Superhydrophobic Surface through an Aerosol-Assisted Chemical Vapor Deposition Process. *Langmuir* **2022**, *38*, 7825–7832.

(5) Jeevahan, J.; Chandrasekaran, M.; Britto Joseph, G.; Durairaj, R. B.; Mageshwaran, G. Superhydrophobic surfaces: a review on fundamentals, applications, and challenges. *J. Coatings Technol. Res.* **2018**, *15*, 231–250.

(6) Ozkan, E.; Garren, M.; Manuel, J.; Douglass, M.; Devine, R.; Mondal, A.; Kumar, A.; Ashcraft, M.; Pandey, R.; Handa, H. Superhydrophobic and Conductive Foams with Antifouling and Oil–Water Separation Properties. *ACS Appl. Mater. Interfaces* **2023**, *15*, 7610–7626.

(7) Liu, Y.; Tan, X.; Li, X.; Xiao, T.; Jiang, L.; Nie, S.; Song, J.; Chen, X. Eco-Friendly Fabrication of Transparent Superhydrophobic Coating with Excellent Mechanical Robustness, Chemical Stability, and Long-Term Outdoor Durability. *Langmuir* **2022**, *38*, 12881–12893.

(8) Chen, W.; Wang, W.; Luong, D. X.; Li, J. T.; Granja, V.; Advincula, P. A.; Ge, C.; Chyan, Y.; Yang, K.; Algozeeb, W. A.; Higgs, C. F.; Tour, J. M. Robust Superhydrophobic Surfaces via the Sand-In Method. *ACS Appl. Mater. Interfaces* **2022**, *14*, 35053–35063.

(9) Zhang, Y.; Wang, T.; Lv, Y. Durable Biomimetic Two-Tier Structured Superhydrophobic Surface with Ultralow Adhesion and Effective Antipollution Property. *Langmuir* **2023**, *39*, 2548–2557.

(10) McHale, G.; Shirtcliffe, N. J.; Newton, M. I. Contact-angle hysteresis on super-hydrophobic surfaces. *Langmuir* **2004**, *20*, 10146–10149.

(11) Gao, L.; McCarthy, T. J. Contact angle hysteresis explained. *Langmuir* **2006**, *22*, 6234–6237.

(12) Guo, X. J.; Xue, C. H.; Sathasivam, S.; Page, K.; He, G.; Guo, J.; Promdet, P.; Heale, F. L.; Carmalt, C. J.; Parkin, I. P. Fabrication of robust superhydrophobic surfaces via aerosol-assisted CVD and thermo-triggered healing of superhydrophobicity by recovery of roughness structures. *J. Mater. Chem. A* **2019**, *7*, 17604–17612.

(13) Huang, J. Y.; Li, S. H.; Ge, M. Z.; Wang, L. N.; Xing, T. L.; Chen, G. Q.; Liu, X. F.; Al-Deyab, S. S.; Zhang, K. Q.; Chen, T.; Lai, Y. K. Robust superhydrophobic TiO<sub>2</sub>@fabrics for UV shielding, self-cleaning and oil-water separation. *J. Mater. Chem. A* **2015**, *3*, 2825–2832.

(14) Dalvi, V. H.; Rossky, P. J. Molecular origins of fluorocarbon hydrophobicity. *Proc. Natl. Acad. Sci. U. S. A.* **2010**, *107*, 13603–13607.

(15) Bayer, I. S. Superhydrophobic Coatings from Ecofriendly Materials and Processes: A Review. *Adv. Mater. Interfaces* **2020**, *7*, 2000095.

(16) Alonso Frank, M.; Meltzer, C.; Braunschweig, B.; Peukert, W.; Boccaccini, A. R.; Virtanen, S. Functionalization of steel surfaces with organic acids: Influence on wetting and corrosion behavior. *Appl. Surf. Sci.* **2017**, *404*, 326–333.

(17) Heale, F. L.; Page, K.; Wixey, J. S.; Taylor, P.; Parkin, I. P.; Carmalt, C. J. Inexpensive and non-toxic water repellent coatings comprising SiO<sub>2</sub> nanoparticles and long chain fatty acids. *RSC Adv.* **2018**, *8*, 27064–27072.

(18) Daneshmand, H.; Sazgar, A.; Araghchi, M. Fabrication of robust and versatile superhydrophobic coating by two-step spray method: An experimental and molecular dynamics simulation study. *Appl. Surf. Sci.* **2021**, *567*, 150825.

(19) Kothary, P.; Dou, X.; Fang, Y.; Gu, Z.; Leo, S. Y.; Jiang, P. Superhydrophobic hierarchical arrays fabricated by a scalable colloidal lithography approach. *J. Colloid Interface Sci.* **2017**, *487*, 484–492.

- (20) Xu, Q. F.; Mondal, B.; Lyons, A. M. Fabricating superhydrophobic polymer surfaces with excellent abrasion resistance by a simple lamination templating method. *ACS Appl. Mater. Interfaces* **2011**, *3*, 3508–3514.
- (21) Xie, L.; Tang, Z.; Jiang, L.; Breedveld, V.; Hess, D. W. Creation of superhydrophobic wood surfaces by plasma etching and thin-film deposition. *Surf. Coat. Technol.* **2015**, *281*, 125–132.
- (22) Meena, M. K.; Sinhamahapatra, A.; Kumar, A. Superhydrophobic polymer composite coating on glass via spin coating technique. *Colloid Polym. Sci.* **2019**, *297*, 1499–1505.
- (23) Wang, S.; Liu, C.; Liu, G.; Zhang, M.; Li, J.; Wang, C. Fabrication of superhydrophobic wood surface by a sol-gel process. *Appl. Surf. Sci.* **2011**, *258*, 806–810.
- (24) Marchand, P.; Hassan, I. A.; Parkin, I. P.; Carmalt, C. J. Aerosol-assisted delivery of precursors for chemical vapour deposition: expanding the scope of CVD for materials fabrication. *Dalt. Trans.* **2013**, *42*, 9406–9422.
- (25) Campbell, S. A.; Smith, R. C. Chemical vapour deposition. *High k Gate Dielectrics* **2003**, *1*, 65–88.
- (26) Bryant, W. A. The fundamentals of chemical vapour deposition. *J. Mater. Sci.* **1977**, *12*, 1285–1306.
- (27) Knapp, C. E.; Carmalt, C. J. Solution based CVD of main group materials. *Chem. Soc. Rev.* **2016**, *45*, 1036–1064.
- (28) Ashraf, S.; Blackman, C. S.; Hyett, G.; Parkin, I. P. Aerosol assisted chemical vapour deposition of MoO<sub>3</sub> and MoO<sub>2</sub> thin films on glass from molybdenum polyoxometallate precursors; thermophoresis and gas phase nanoparticle formation. *J. Mater. Chem.* **2006**, *16*, 3575–3582.
- (29) Tombesi, A.; Li, S.; Sathasivam, S.; Page, K.; Heale, F. L.; Pettinari, C.; Carmalt, C. J.; Parkin, I. P. Aerosol-assisted chemical vapour deposition of transparent superhydrophobic film by using mixed functional alkoxysilanes. *Sci. Rep.* **2019**, *9*, 7549.
- (30) Beamson, G.; Briggs, D. High Resolution XPS of Organic Polymers: The Scienta ESCA300 Database. *J. Chem. Educ.* **1993**, *70*, A25.
- (31) Chao, S. S.; Takagi, Y.; Lucovsky, G.; Pai, P.; Custer, R. C.; Tyler, J. E.; Keem, J. E. Chemical states study of Si in SiO<sub>x</sub> films grown by PECVD. *Appl. Surf. Sci.* **1986**, *26*, 575–583.
- (32) Sun, L.; Han, C.; Wu, N.; Wang, B.; Wang, Y. High temperature gas sensing performances of silicon carbide nanosheets with an n-p conductivity transition. *RSC Adv.* **2018**, *8*, 13697–13707.
- (33) Osman, M. A.; Suter, U. W. Surface treatment of calcite with fatty acids: Structure and properties of the organic monolayer. *Chem. Mater.* **2002**, *14*, 4408–4415.
- (34) Kapridaki, C.; Maravelaki-Kalaitzaki, P. TiO<sub>2</sub>-SiO<sub>2</sub>-PDMS nano-composite hydrophobic coating with self-cleaning properties for marble protection. *Prog. Org. Coatings* **2013**, *76*, 400–410.
- (35) Li, Y.; Zhang, B. P.; Zhao, C. H.; Zhao, J. X. Structure transition, formation, and optical absorption property study of Ag/SiO<sub>2</sub> nanofilm by sol-gel method. *J. Mater. Res.* **2012**, *27*, 3141–3146.
- (36) Lathe, S. S.; Imai, H.; Ganesan, V.; Rao, A. V. Superhydrophobic silica films by sol-gel co-precursor method. *Appl. Surf. Sci.* **2009**, *256*, 217–222.
- (37) Socrates, G. *Infrared and Raman Characteristic Group Frequencies: Tables and Charts*, 3rd ed.; John Wiley & Sons Inc., New York, 2004; pp 366–400.
- (38) Roach, P.; Shirtcliffe, N. J.; Newton, M. I. Progress in superhydrophobic surface development. *Soft Matter* **2008**, *4*, 224.
- (39) Xu, Q. F.; Liu, Y.; Lin, F. J.; Mondal, B.; Lyons, A. M. Superhydrophobic TiO<sub>2</sub>-polymer nanocomposite surface with UV-induced reversible wettability and self-cleaning properties. *ACS Appl. Mater. Interfaces* **2013**, *5*, 8915–8924.
- (40) Zhu, X.; Zhang, Z.; Men, X.; Yang, J.; Xu, X.; Zhou, X. Plasma/thermal-driven the rapid wettability transition on a copper surface. *Appl. Surf. Sci.* **2011**, *257*, 3753–3757.
- (41) Chen, F.; Wang, Y.; Tian, Y.; Zhang, D.; Song, J.; Crick, C. R.; Carmalt, C. J.; Parkin, I. P.; Lu, Y. Robust and durable liquid-repellent surfaces. *Chem. Soc. Rev.* **2022**, *51*, 8476–8583.